

ARTICLE

<https://doi.org/10.1038/s42004-019-0144-1>

OPEN

Direct quantification of surface barriers for mass transfer in nanoporous crystalline materials

Mingbin Gao^{1,2}, Hua Li¹, Miao Yang¹, Shushu Gao^{1,2}, Pengfei Wu^{1,2}, Peng Tian¹, Shutao Xu¹, Mao Ye¹ & Zhongmin Liu¹

Mass transfer of guest molecules in nanoporous crystalline materials has gained attention in catalysis, separation, electrochemistry, and other fields. Two mechanisms, surface barriers and intracrystalline diffusion, dominate the mass transport process. Lack of methods to separately quantify these two mechanisms restricts further understanding and thus rational design and efficient application of nanoporous materials. Here we derive an approximate expression of uptake rate relying solely on surface permeability, offering an approach to directly quantify surface barriers and intracrystalline diffusion. By use of this approach, we study the diffusion in zeolitic materials, and find that the intracrystalline diffusivity is intrinsic to the topological structure of host materials at low molecular loading for the given guest molecules, while the surface permeability is sensitive to the non-ideality of a crystalline surface owing to the physical and chemical properties of the crystalline surface, host-guest interaction at the surface, and change of the environment.

¹National Engineering Laboratory for Methanol to Olefins, Dalian National Laboratory for Clean Energy, iChEM (Collaborative Innovation Center of Chemistry for Energy Materials), Dalian Institute of Chemical Physics, Chinese Academy of Sciences, 116023 Dalian, China. ²University of Chinese Academy of Sciences, 10049 Beijing, China. These authors contributed equally: Mingbin Gao, Hua Li. Correspondence and requests for materials should be addressed to M. Ye (email: maoye@dicp.ac.cn) or to Z.L. (email: liuzm@dicp.ac.cn)

The past decades saw the rapid development and utilization of nanoporous crystalline materials in a wide variety of scientific researches and industrial processes^{1–11}. Typical applications are, but not limited to, catalysis^{1–4}, separation^{5–7}, and electrochemistry⁸. Efficient design and successful application of nanoporous crystalline materials are essentially dependent on the molecular transport properties because of the constraints of mass transfer in these processes^{12,13}. Nevertheless, the theoretical picture of molecular transport in nanoporous materials is still incomplete and remains elusive^{6,14}. For long time, intracrystalline diffusion has been recognized as the dominant mechanism controlling mass transfer in nanoporous materials^{12,15}. However, studies based on the visualization methods such as interference microscopy (IFM) and infrared microscopy (IRM) discovered that, in addition to intracrystalline diffusion, surface barriers can also dominate the mass transfer of guest molecules in some nanoporous materials^{3,12,16}. Recently, Weckhuysen et al.^{17,18} developed a fluorescence microscopy approach to directly observe the diffusion behavior in porous materials. It is shown that the diffusivity derived from the commonly used uptake/release rate measurement is in fact the apparent diffusivity reflecting the combined influence of intracrystalline diffusion and surface barriers in the nanoporous crystalline materials^{6,15,19,20}. The crystal size^{6,21–23}, hierarchical pores^{24–27}, surface modifications^{16,28}, etching^{29,30}, and post-processing^{5,31,32} can alter surface barriers, own to different underlying mechanisms such as surface defects, guest molecule inhibition, pore restriction, surface adsorption, or desorption, etc., and thus change the overall mass transfer rate, which can eventually affect the product selectivity in catalytic reaction^{28,33,34} and the efficiency in separation process^{6,7}. The originality of surface barriers, though not being fully understood, can be partially attributed to surface defects (e.g. pore blockage, mismatch in pore alignment, and silicalite outer crust)^{15,35,36}, guest-host interaction at the surface^{26,27,37}, and/or the combination of these two effects²⁴, as schematically shown in Fig. 1a. Meanwhile, based on the transition state theory^{23,38}, the intracrystalline diffusivity is directly related to the properties of guest molecules and the structure of host nanoporous crystalline materials^{14,38}, and thus it should be independent of measurement techniques, crystal size, and external surface characteristics. In view of the different physical originalities of surface barriers and intracrystalline diffusion, direct quantification of these two mechanisms is highly desired to identify the limitations of mass transfer, and optimize the design and utilization of nanoporous crystalline materials.

IFM and IRM techniques provide the possibility to quantify the surface barriers and intracrystalline diffusion in nanoporous crystalline materials via the profile of concentration of guest

molecules cross a single crystal^{3,12,39}. However, these microscopy techniques, constrained by low spatial resolution, are limited to observe the nanoporous materials with large crystal size (>20 μm), good optical transparency, and well-defined structure³. However, the synthesis of nanoporous crystal larger than 20 μm is usually time-consuming and requires harsh experimental conditions⁴⁰. Moreover, in practice, nanoporous materials are composed of crystals with size from nanoscale to a few microns in order to maximize turnover and active sites accessibility^{33,41}. Therefore, a generic method for direct quantifying the surface barriers and intracrystalline diffusion in nanoporous materials with small crystals of practical interests needs to be developed.

In principle, the uptake/release rate, if fitted with the dual-resistance model (DRM), can be used to quantify the surface barriers and intracrystalline diffusion^{42,43}. DRM is a modified version of the intracrystalline diffusion model in which the effect of surface barriers is incorporated. The uptake/release rate can be readily measured by many conventional techniques, for example, intelligent gravimetric analyzer (IGA)²⁵, tapered element oscillating microbalance (TEOM)^{19,44}, TA instruments⁴⁵, quartz crystal microbalance (QCM)⁵, and fast time-resolved Fourier transform infrared spectroscopy (FTIR)^{28,33}. The uptake/release rates measured by these techniques are not constrained by crystal size, optical transparency, structure, and surface morphology of the materials. Quantifying surface barriers (or intracrystalline diffusion) via this approach, however, requires in prior and quantitative information of intracrystalline diffusivity (or surface permeability) in the nanoporous materials^{3,22}. Based on the uptake/release rate measurement, Heinke et al.⁵ proposed to obtain the intracrystalline diffusivity and surface permeability using the relation between the characteristic time of overall mass transport and crystal size of materials. Nevertheless, such method requires the preparation of crystalline materials with a series of crystal sizes and is difficult to quantify the mass transport properties of a specific material in practice. Fasano et al.⁶ derived the intracrystalline diffusivity by molecular dynamics (MD) simulations, and attributed the discrepancy between the apparent diffusivity and MD results to the effect of surface barriers. In fact, the intracrystalline diffusivity derived from MD simulations may differ from that in real materials as highly simplified configuration is normally used to reduce the computational cost. Besides, direct experimental validation of the MD results is difficult, since the self-diffusivity can only be measured by advanced techniques such as pulsed field gradient (PFG) nuclear magnetic resonance (NMR).

Here, we show an approximate expression of uptake rate relying solely on surface permeability (see Fig. 1b). This provides a method to directly quantify the surface barriers (and

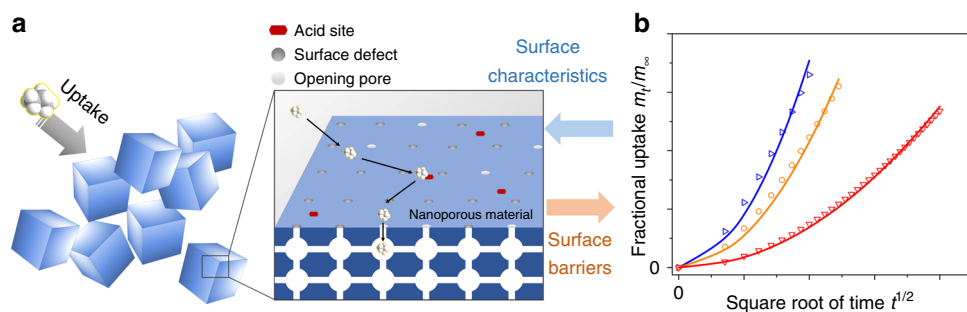


Fig. 1 Scheme for quantifying surface permeability from uptake rate measurement. **a** A ‘detour’ of guest molecules on external surface is determined by surface characteristics, which causes additional surface diffusion paths and enhanced surface barriers. **b** By use of our developed method, i.e., Eq. (3), the surface permeability could be directly quantified from the uptake rate measurements. The scatters are obtained from the uptake rate measurements while solid lines are fitting results by Eq. (3), and the effect of surface barriers is enhanced with the solid lines in colors in the order of blue, orange, and red

intracrystalline diffusivity) in nanoporous materials, in which neither the prior information of intracrystalline diffusion nor crystal size (or morphology) possesses the constraints. Thus, the effects of surface barriers and intracrystalline diffusion may be identified separately.

Results

Explicit expression of uptake rate with surface permeability. The relative uptake loading m_t/m_∞ of guest molecules in a plane sheet can be described by^{42,43}

$$\frac{m_t}{m_\infty} = 1 - \sum_{n=1}^{\infty} \frac{2L^2 \exp\left(-\frac{\beta_n^2 Dt}{l^2}\right)}{(\beta_n^2 + L^2 + L)\beta_n^2}; \beta_n \tan \beta_n = L \quad (1)$$

where m_t/m_∞ is the relative uptake loading of guest molecules, t the uptake time, l the half thickness of the plane sheet, i.e., characteristic length of the intracrystalline diffusion⁶, D the intracrystalline (transport) diffusivity, α the surface permeability, and $L = \alpha l/D$ the ratio of characteristic time of intracrystalline diffusion to that of surface barriers. It is hard to fit the DRM model represented by Eq. (1) to simultaneously quantify the surface barriers and intracrystalline diffusion without in prior information of either surface barriers or intracrystalline diffusion^{3,22}. A solution could be obtained for sufficiently small t based on the Laplace transform⁴²

$$\frac{m_t}{m_\infty} \Big|_{t \rightarrow 0} = \sqrt{\frac{4Dt}{\pi l^2}} - \frac{1 - \exp\left(L^2 \frac{D}{l^2} t\right) \operatorname{erfc}\left(L \sqrt{\frac{Dt}{l^2}}\right)}{L} \quad (2)$$

Though Eq. (1) has been significantly simplified to Eq. (2), it still contains the contribution of both surface barriers and intracrystalline diffusion. Expanding Eq. (2) by Taylor series of variable \sqrt{t} (see Supplementary Note 1), we obtain

$$\frac{m_t}{m_\infty} \Big|_{\sqrt{t} \rightarrow 0} \cong \frac{\alpha}{l} (\sqrt{t})^2 + O(\sqrt{t^3}) \quad (3)$$

As can be seen, in Eq. (3) the relative loading m_t/m_∞ is actually a quadratic function of square root of uptake time, \sqrt{t} . Interestingly, the quadratic coefficient only relies on the surface permeability and the characteristic length of intracrystalline diffusion, which opens an approach to directly quantify the surface barriers based on the uptake/release rate. Note that Eq. (3) is derived based on the plane sheet. In practice, nanoporous crystalline materials can be in different shapes, such as sphere, cube, and many others. Thus, we propose an equivalent characteristic length of the intracrystalline diffusion for different shapes based on the characteristic time of intracrystalline diffusion⁴⁶, which can be readily derived^{3,19,22}

$$\tau_{\text{diff, slab}} = \frac{l^2}{3D}; \tau_{\text{diff, sphere}} = \frac{R^2}{15D}; \tau_{\text{diff, cube}} = \frac{(a/2)^2}{12.3956D} \quad (4)$$

where R is the radius of a spherical crystal, and a the length of a cubic crystal. The equivalent lengths for, respectively, spherical and cubic crystals are

$$l = \frac{R}{\sqrt{5}}, l = \frac{(a/2)}{2.03} \quad (5)$$

Equation (3), together with Eq. (5), can be applied to determine surface permeability α in nanoporous crystalline materials with different shapes by use of initial uptake/release rate. In doing so, Eq. (3) is first used to fit the measured uptake/release rate data at the time interval $0 \sim \sqrt{t}$, and the corresponding coefficient of determination of Eq. (3) is estimated. An optimal $\sqrt{t^*}$ is chosen based on the maximum coefficient of determination, and α corresponding to time interval $0 \sim \sqrt{t^*}$ is considered as the approximation of surface permeability. The intracrystalline

diffusivity D can be subsequently obtained by fitting the whole uptake/release rate data with DRM, as represented by Eq. (1), since the surface permeability α is known. Compared to the method based on DRM with both D and α as free parameters, our proposed approach can significantly reduce the uncertainty of the fitting results (see Supplementary Note 2).

An analysis has been conducted to understand the applicable range of Eq. (3) (see Supplementary Note 3). It is found that, when L is large than 120, the mass transfer in nanoporous materials is dominated by intracrystalline diffusion⁴⁷, and it is hard to reliably derive surface permeability via the Eq. (3). When L is lower than 120, the surface permeability can be well predicted by Eq. (3). Note that for $L < 120$ the temporal resolution for the uptake rate measurement is about ~ 1 s, it is in the range that most of common-used apparatuses such as TA, IGA, TEOM, and IR spectroscopy can achieve^{3,6,19,22,48}.

In practical applications, uptake rate measurements are usually performed with a bed of crystals. Considering the crystals in the bed may have different size and surface permeability³, we derived Eq. (6) to describe the surface permeability of a bed of crystals (see Supplementary Note 4):

$$\frac{m_t}{m_\infty} \Big|_{\sqrt{t} \rightarrow 0} \cong \sum_i^n \left(\frac{\omega_i}{l_i} \alpha_i \right) (\sqrt{t})^2 \quad (6)$$

where n is the number of crystals in the bed, and ω_i is the volume fraction of the i th crystal with corresponding length l_i . Careful check of the Eqs. (3) and (6) suggests that the surface permeability determined by Eq. (3) in experiments with a bed of crystals is actually an average over diverse crystals. This may possess another limitation for our proposed method, that is, it is only suitable for samples with a narrow crystal size distribution. This can normally be achieved through the control of synthesis procedures and conditions, as well as physical sieving^{3,48}. The relation between the surface permeability of an individual crystal and that of a bed of crystals is subjected to a further investigation.

The characteristic time of overall mass transport τ_{eff} can be regarded as the sum of the contributions from intracrystalline diffusion and surface barriers⁶: $\tau_{\text{eff}} = \tau_{\text{diff}} + \tau_{\text{surf}}$. Note that τ_{eff} can be connected to the effective (or apparent) diffusivity D_{eff} ^{3,5,6}

$$\frac{1}{D_{\text{eff}}} = \frac{1}{D} + \frac{3}{\alpha l} \quad (7)$$

which lumps together possible influences of transport resistances for nanoporous materials.

Methanol diffusion in SAPO-34 measured by various techniques.

A challenge in the study of mass transfer in nanoporous materials is the large deviation of intracrystalline diffusivity obtained by different measurement techniques^{12,19}. We revisited the uptake rate of methanol in SAPO-34 zeolites measured by three typical techniques, i.e., IFM³, IGA (this work), and TEOM⁴⁴, by use of our developed method. For comparison, PFG NMR measurement at small molecular loading was performed to derive intracrystalline self-diffusivity of methanol in SAPO-34 zeolites (see Supplementary Method). As shown in Fig. 2a, the effective diffusivities measured by three different techniques span over two orders of magnitude. After decoupling the surface barriers from overall mass transfer resistance by Eq. (3), we can obtain intracrystalline (transport) diffusivities based on three different measurement techniques, which include both macro- (IGA and TEOM) and micro- (IFM) methods. As can be seen in Fig. 2a, the intracrystalline (transport) diffusivities show surprising consistence, which are about 1.06×10^{-12} m²/s. Beerdse et al.³⁸ and Chmelik et al.⁴⁹ identified that, at sufficiently low molecular loading, the intracrystalline diffusivity of guest

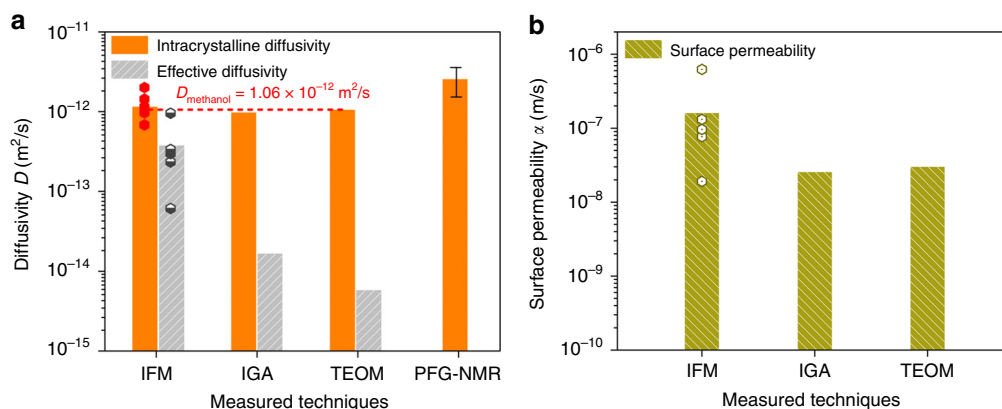


Fig. 2 Diffusion of methanol in SAPO-34 zeolites measured by different techniques. **a** The comparison between intracrystalline diffusivity and effective diffusivity of methanol in SAPO-34 zeolites at 303 K by different measured techniques. Intracrystalline (transport) diffusivity is obtained by DRM shown as Eq. (9) with surface permeability obtained in **b** for IFM³ (0 → 1 mbar), IGA (0 → 0.6 mbar) and TEOM⁴⁴ techniques. Intracrystalline self-diffusivity is obtained by Supplementary Eq. 30 for PFG NMR (ca. fractional occupancy 0.08). Effective diffusivity is calculated by Eq. (7). The error bar is $\pm 1.01 \times 10^{-12} \text{ m}^2/\text{s}$. The scatters for IFM are results of individual crystals. **b** The surface permeability of methanol in SAPO-34 zeolites at 303 K measured by different techniques. The scatters for IFM are results of individual crystals. The surface permeability is obtained via Eq. (3)

molecules is determined by the passage through the micropore rather than by drag effects with other molecules. Therefore, at the small molecular loading, the intracrystalline self-diffusivity and transport diffusivity are coincide. As shown in Fig. 2a, the intracrystalline self-diffusivity of methanol in SAPO-34 zeolites at sufficiently small methanol loading (ca. fraction occupancy 0.08) agrees well with the transport diffusivities measured by three different techniques. This means that after decoupling surface barriers from overall mass transfer by Eq. (3), the intracrystalline diffusivities obtained by different approaches can be unified. As discussed above, the intracrystalline diffusivity is mainly related to the properties of guest molecules, the nanoporous structure of the host materials, and the corresponding guest-host interaction. Though different measurement techniques are used, for the given guest molecules (i.e., methanol), the intracrystalline diffusivities measured by these four techniques agree well, suggesting that intracrystalline diffusivity is indeed intrinsic to the topological structure of host materials.

Figure 2b shows that the surface permeabilities measured by three different techniques. As shown, the surface permeability changes to certain extent when different techniques are used, which may be resulted from the difference between the samples used, as there are many different physical reasons (for example, surface defects³⁵, surface adsorption or desorption^{24,27}, and surface composition³¹) that might cause surface barriers. One of the potential reasons may be due to different Si content of the SAPO zeolites used in the measurements, as shown by Tzoulaki et al.³¹ and our experimental results in this work (see Supplementary Fig. 16). For the results of surface permeability by IFM, it was shown that such discrepancy could be due to the external surface characteristic of individual crystal, such as Si content³¹ or local surroundings³. As depicted in Supplementary Fig. 16a, increasing Si content of SAPO-34 would lead to surface permeability decrease, which may be resulted from higher adsorption frequency by increased surface acidity. Therefore, the deviation between the surface permeability measured by IGA and TEOM may also partly result from different Si content of SAPO-34 zeolites used, which are about 0.084 and 0.079, respectively⁴⁴. Nevertheless, the gap between the surface permeability of individual crystallites and crystallite assemblages still needs to be further investigated. In addition, the effects of chemical content and experimental conditions (such as storage^{5,31} and activation protocol)³¹ cannot be completely excluded.

From this case, notably, it reveals that the discrepancy of effective diffusivities obtained by different uptake measurement techniques mainly results from the effect of surface barriers. Our proposed method indeed provides a tool to directly determine surface permeability and intracrystalline diffusivity, which is not constrained by measurement techniques.

Propane diffusion in SAPO-34 of different size and acidity.

The uptake rates of propane in SAPO-34 zeolites with different crystal size (average size ca. 0.05, 0.50, 1.00, 3.50, 8.00 μm) were measured by IGA, which are shown in Fig. 3a. We then quantified the surface permeability α by fitting the initial uptake rate with Eq. (3), as shown in Fig. 3b. Based on the obtained surface permeability α , we further fitted the whole uptake rate data (as shown in Fig. 3a) with Eq. (9) and derived the intracrystalline diffusivity D , which is shown in Fig. 3d. For comparison, in Fig. 3d, we also show the effective diffusivity of propane in SAPO-34 zeolites calculated by Eq. (7). It is found that the effective diffusivity decreases by two orders of magnitude as the crystal size decreases from 3.50 μm to 0.05 μm . Based on the transition state theory^{23,50}, the intracrystalline diffusivity is mainly dependent on the interaction between specific guest molecule and host materials. Furthermore, Monte Carlo simulations also verified that intracrystalline diffusivity is independent of crystal size^{21,37,51}. As can be seen in Fig. 3d, the derived intracrystalline diffusivity is almost invariant with the change of crystal size.

From Eq. (7) we can deduce that, as the size of crystal decreases, the contribution of surface barriers to mass transfer resistance may become more and more significant compared to that of intracrystalline diffusion. The almost constant intracrystalline diffusivity for different crystal size as shown in Fig. 3d actually suggests that the change of effective diffusivity of propane might be mainly due to the effect of surface barriers. In Fig. 3e we compared α of propane for two groups of samples: one is the sample SAPO-34-3.5 and SAPO-34-8, and the other is the samples SAPO-34-0.5 and SAPO-34-1.0 (Si-0.16). Each group of samples has different crystal size but close density of external acidity. As can be seen, α is almost invariant for each group of samples. According to the Monte Carlo simulation by Teixeira et al.²¹, the surface permeability is independent of crystal size, which, however, is strongly dependent on the surface characteristics. To gain further insight into surface interaction, we

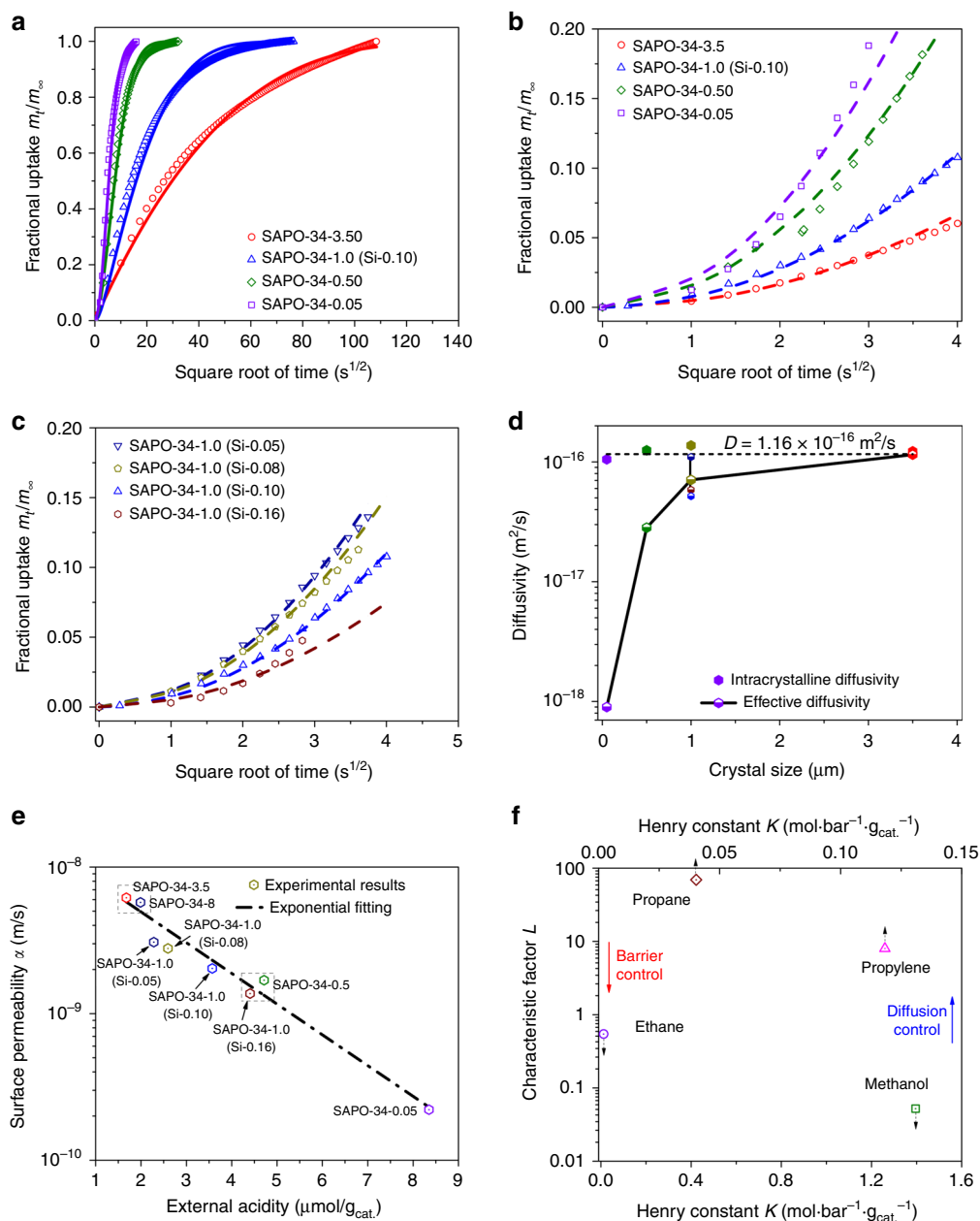


Fig. 3 Uptake of propane in SAPO-34 zeolites with different crystal size and Si content. **a** Uptake rate of propane in SAPO-34 zeolites with different crystal size measured by IGA at 313 K (0 → 9 mbar). The scatters represent the experimental data while solid lines are fitting results by Eq. (9). **b, c** Initial uptake rate of propane in SAPO-34 zeolites with different crystal size and Si content. The scatters represent the experimental data while dash lines are fitting results by Eq. (3). **d** Intracrystalline diffusivities obtained by DRM represented by Eq. (9) with surface permeabilities shown in **e**. Effective diffusivities (half filled scatters) are results calculated by Eq. (7) with intracrystalline diffusivities shown in this figure and surface permeabilities shown in **e**. **e** The change of surface permeabilities with regard to the external acidity of SAPO-34 zeolites. The surface permeability is obtained via Eq. (3) via the data in **b, c**. An exponential function (dash dot line) is used to fit the relation between surface permeability and external acidity of SAPO-34 zeolites. **f** The relation between characteristic factor L and Henry's constant K of different guest molecules (methanol, ethane, propylene and propane) at 313 K

measured the uptake rates of propane in SAPO-34 with similar size but different Si content. As shown in Fig. 3c, the initial uptake rate shows a distinct deceleration as the Si content increases. We thus calculated α by use of Eq. (3). Note that the density of external acidity on the surface is closely related to the Si content of SAPO-34 (see Supplementary Fig. 16). It is speculated the slow of surface permeability may be directly related to the increased density of external acidity at the surface. As can be seen from Fig. 3e, α shows an exponentially decrease with increasing external acidity (see Supplementary Method). Based on the surface defects mechanism^{15,20,21,35}, guest molecules need to take

a detour on the external surface of nanoporous materials to find pore entrances. Higher density of acid sites would lead to more frequent interaction between acid sites and guest molecules, which then causes the slow surface permeability of guest molecules. Therefore, we deduce that the originality of this acidity-dependent surface permeability in SAPO-34 zeolites is attributed to the different interaction frequency between external acidity and guest molecules.

In order to further understand that surface interaction can affect surface barriers, the uptake rates of two groups of tracers, i.e., methanol with ethane (kinetic diameter ~ 4.0 Å) and

propylene with propane (kinetic diameter ~ 4.4 Å), were measured. Each group of tracers have similar molecular size but different surface interaction strengths. We calculated the surface permeability and intracrystalline diffusivity of each tracer in SAPO-34 zeolites by use of our proposed method. The intracrystalline diffusivity of ethane is about 1.25×10^{-12} m²/s (ca. fractional occupancy 0.035), which agrees with the measured results ($\sim 10^{-12}$ m²/s) by PFG NMR⁵². In Fig. 3f, the Henry's constants of these molecules are used to reflect the interaction strength between guest molecules and surface of host materials (see Supplementary Fig. 14). As can be seen, for similar molecular size, L decreases when Henry's constant increases. This means that the importance of surface barriers in mass transfer increases when Henry's constant becomes higher, i.e., the interaction between guest molecules and external surface of host materials is enhanced. In other words, both higher density of external acidity and stronger surface interaction might slow the surface permeability of guest molecules in mass transfer in SAPO-34 zeolites, which is not entirely dependent on the peculiar mechanisms of molecular transport.

Propane diffusion in SAPO-34 when exposed to humid air. To obtain a better understanding of the impact of environmental conditions on surface barriers^{5,31,32,53}, we investigated the uptake rate of propane in SAPO-34 zeolites absorbed different quantity of water vapor and exposed to humid air for different time. Tzoulaki et al.³² found that the presence of water would retard the surface permeability in MFI zeolites via IFM measurements. Heinke et al.^{5,54} found that preferential surface degradation of MOF film upon exposure to humid air can cause surface barriers, although the changes in crystallinity were minor. However, in the work of Heinke et al., the changes in surface permeability were not directly quantified. Therefore, the role of water, i.e., causing steric hindrance and/or structure degradation, in surface barriers is still unclear. We first studied the effect of water steric hindrance by measuring uptake rate of propane in SAPO-34 zeolites adsorbed with different quantities of water. The water-adsorbed SAPO-34 zeolites were prepared by exposing the samples to water vapor at the different pressure under 313 K for 1 h in IGA apparatus. Assuming that the changes of concentration of water in zeolites are negligible at the initial uptake stage of uptake measurement, the initial uptake process are mainly attributed to the uptake of propane. As shown in Fig. 4a, when the quantity of adsorbed-water in SAPO-34 increases, the initial uptake rate of propane reduces significantly. Figure 4d shows α calculated via Eq. (3). As can be seen, the adsorbed-water in SAPO-34 zeolites significantly retards the surface permeability. As the adsorption of water might also cause structure degradation, we examined the structure degradation of SAPO-34 zeolites pre-adsorbed saturated water vapor at 313 K for 1 day. This sample was outgassed under 623 K for 6 h before the propane uptake rate measurement (see Supplementary Fig. 15). Even for a short exposure time (1 day), as shown in Fig. 4d, adsorption of water can cause structure degradation in SAPO-34 zeolites, which can also lead surface permeability to decrease. But as shown in Fig. 4d, the water hindrance, compared to the structure degradation, is the dominant factor causing the surface barriers in SAPO-34 zeolites exposing to water for short time.

We then studied the effect of structure degradation on the surface permeability in SAPO-34 zeolites by exposing the samples to humid air with about 30% moisture at 298 K for 0.1, 1, 3, and 5 months, respectively. Before uptake rate measurements, these aged samples were outgassed at 623 K for at least 6 h to minimize the impact of adsorbed-water. As observed in Fig. 4b,c, prolonging the exposure time to humid air can lead to

a significant retardation of the uptake rate of propane. It is shown in Fig. 4e that, when the SAPO-34 zeolites have been exposed to air for five months, α decreases by a factor of ~ 20 , and meanwhile the intracrystalline diffusivity only decreases by a factor of ~ 4.5 . Careful check with Fig. 4e indicates that α drops rapidly when SAPO-34 zeolites were initial exposed to humid air, and then reaches an equilibrium value after about 3 months. The intracrystalline diffusivity, however, manifests a relatively steady decrease as the time of exposure increases. Li et al.⁵⁵ demonstrated that when SAPO-34 zeolites exposed to moisture at room temperature, the hydrolysis can affect acidity and causes defects in SAPO-34 zeolites. Therefore, further revealing the changes of chemical environment and structure defects in external surface of SAPO-34 zeolites exposed to humid air is necessary. Figure 4f shows that the concentration of external acidity increases with exposure time, and α manifests approximately an exponential decrease with the external acidity. Although detailed characterization of pore blockage in crystalline surface is still challenging, we approximately calculated the fractional of unblocked surface pore^{5,15}. As shown in Fig. 4f, with an increasing exposure time to air increasing, the fractional of unblocked surface pore significantly decreases. We have carefully checked the crystallinity of these aged samples by XRD and found the crystallinity slightly decreases (see Supplementary Fig. 3). We also measured the textural properties by adsorption of nitrogen (see Supplementary Table 2), which demonstrates a minor decrease compared to the pristine samples. The above results confirm that, when SAPO-34 zeolites are exposed to humid air for a long time, the structure degradation first occurs in the external surface and leads to a rapid drop of surface permeability. The structure degradation inside the crystals, however, is slow and stable, which causes a relatively steady decrease of intracrystalline diffusivity of guest molecules. These results suggest that clean and particularly water-free storage conditions are crucial for maintaining SAPO-34 zeolites with high mass transfer rates.

2-methylhexane diffusion in SAPO-11 of varying morphology. Surface properties of nanoporous crystalline materials have crucial impact on surface barriers^{5,15,21,28,33}. As a result, surface modification and post-processing could alter the mass transfer rate of guest molecules. It is commonly accepted that a S-shape of uptake curves were found in the many studies when plotted versus the square root of time, and some attributed this to the effect of surface barriers^{3,16,22,25,29}. Jin et al.²⁵ synthesized a series of SAPO-11 hierarchical zeolites with diverse morphologies with similar crystal size by using different growth modifiers, and speculated that the S-shape uptake curves (see Supplementary Figs. 17–18) were affected by surface barriers. However, lack of direct quantification method for surface barriers makes it only possible to compare the results of the effective diffusivity²⁵. In addition, due to the nanoscale crystal size of these hierarchical materials, it is impractical to determine surface permeability by the use of visualization methods such as IFM and IRM^{3,12}. In this work, we re-visited the results of uptake rate measurement by Jin et al.²⁵ by use of our proposed method. As shown in Fig. 5a, the deviation of the effective diffusivity and intracrystalline diffusivity (both normalized by l^2) is about three orders of magnitudes. Interestingly, even for different surface morphologies, the obtained intracrystalline diffusivities of 2-methylhexane in SAPO-11 hierarchical zeolites are almost invariant, due to the inherent topology structure of SAPO-11 zeolites. As can be seen from Fig. 5b, surface permeability shows a strong correlation with

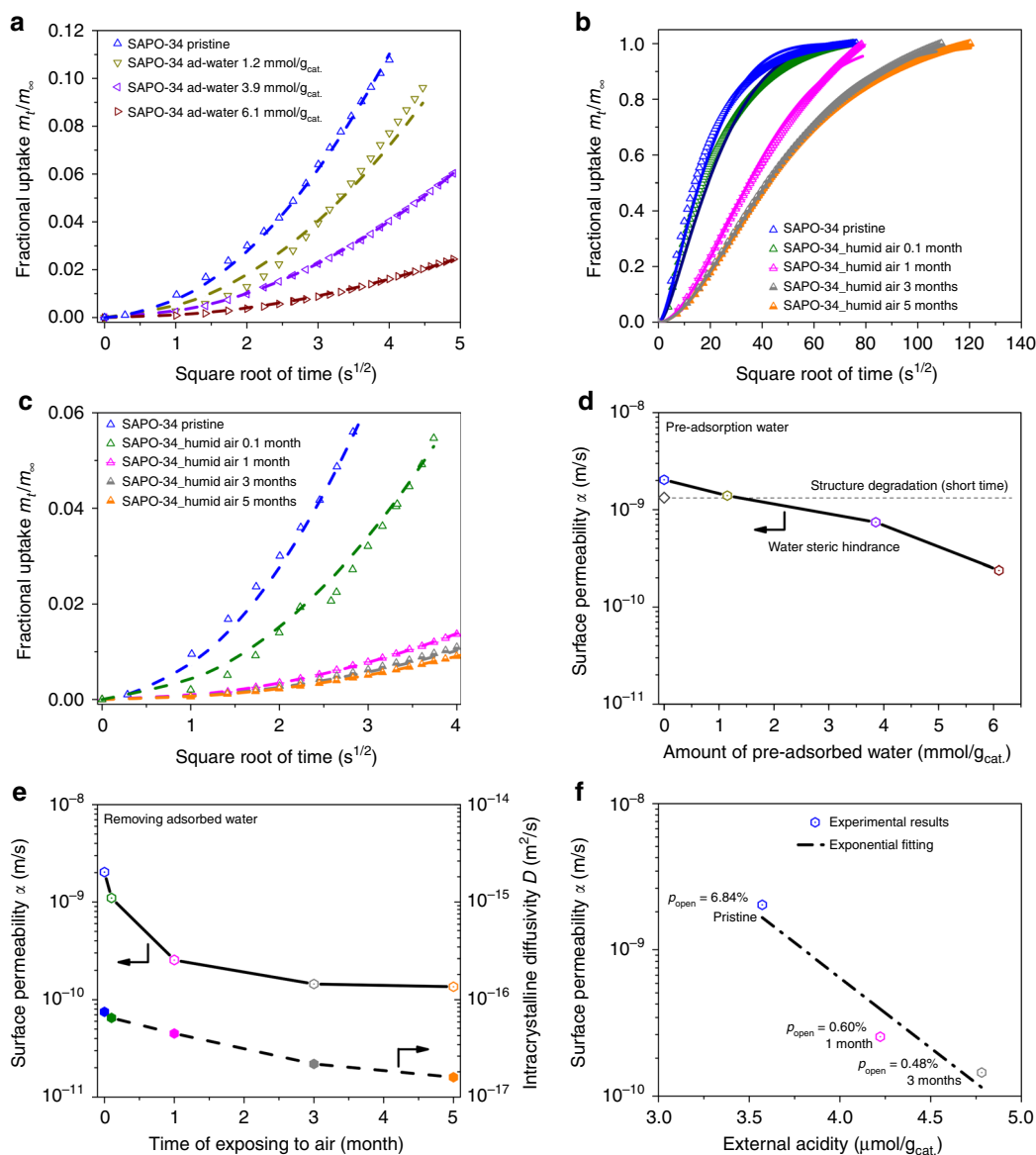


Fig. 4 Uptake of propane in SAPO-34 zeolites after pre-adsorption of water and exposing to air. **a** Uptake of propane in SAPO-34 zeolites with different quantity of adsorbed-water measured by IGA at 313 K (0 → 9 mbar). Surface permeability (dash lines) was derived by Eq. (3). **b** Uptake rate of propane in SAPO-34 zeolites after exposing to air (298 K) for 0.1, 1, 3 and 5 months measured by IGA at 313 K (0 → 9 mbar), the aged samples were outgassed before uptake measurements, fitting with DRM shown as Eq. (9) (solid lines). **c** Initial uptake rate of propane in **b**. **d** The relation between surface permeability of propane and quantity of adsorbed-water. The rhombus represents that the sample was pre-adsorbed saturated water vapor at 313 K for 1 day then outgassed. **e** The relation between intracrystalline diffusivity/surface permeability of propane and exposure time to humid air. **f** The change of surface permeabilities with regard to the external acidity of SAPO-34 zeolites exposed to air for different time, p_{open} denoting the fraction of unblocked surface pore. An exponential function (dash dot line) is used to fit the relation between surface permeability and external acidity of SAPO-34 zeolites

surface morphology. We further analyzed the results by Jin et al.²⁵, and found that the surface permeability actually shows a monotonical decrease with the increased acidity of external surface except for the PDDA case, as shown in Fig. 5b. Heinke et al.¹⁵ argued that the guest molecules need to detour on the external surface to find pore entrances, which are forced to take in order to fill the whole channel system. The surface barriers are caused by the surface properties or geometry rather than the particular mechanisms of molecular transport. When guest molecules take a detour on the external surface of nanoporous materials with high density of acidity, there is a high frequency of interaction between guest molecules and acid sites on external surface, in which case high density of acid sites would retard the surface permeability. Moreover, this

mechanism of surface barriers is also supported implicitly by some investigations. Tzoulaki et al.³¹ found that surface permeability of methanol decreases strongly with increasing Si content (i.e., high acidity) in SAPO STA-7 zeolites by IFM. Fasano et al.⁶ found that high ratio of Al/Si (i.e., high acidity) cause an exponential decrease in surface permeability of water in MFI membranes. Analogously, Zheng et al.⁵⁶ used dealumination and alumination to modify the external surface of H-ZSM-5, and found that relative high ratio of Al/Si can result in the decrease of effective diffusivity of *o*-xylene. In this case, we further substantiate that higher density of external acidity could retard the surface permeability in SAPO-11 zeolites. Therefore, we deduced that external acidity of SAPO zeolites is also a significant factor affecting surface barriers.

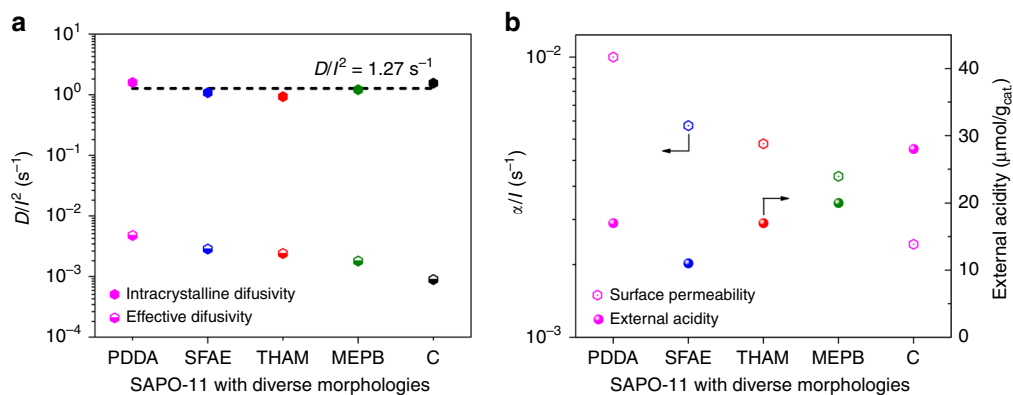


Fig. 5 Uptake of 2-methylhexane in SAPO-11 hierarchical zeolites. **a** The comparison of the effective diffusivity and intracrystalline diffusivity (normalized by l^2) of 2-methylhexane in SAPO-11 hierarchical zeolites with various morphologies at 288 K. Intracrystalline diffusivity is obtained by DRM in Eq. (1) with determined surface permeability shown in **b**. Effective diffusivity is obtained from Jin et al.²⁵ **b** Surface permeability and external acidity of SAPO-11 hierarchical zeolites with various morphologies. The surface permeability is obtained via Eq. (3)

Discussion

Nanoporous crystalline materials are widely used in catalysis, separation, electrochemistry, and among other processes. Two mechanisms, i.e., surface barriers and intracrystalline diffusion, which have different physical originalities, may dominant the mass transport process of guest molecules. In the previous studies, due to lack of methods to direct quantify these two mechanisms, surface barriers and intracrystalline diffusion are often undistinguished in mass transfer of guest molecules^{5,6,22}. The approximate expression of uptake/release rate, which only relies on the surface permeability, can provide an effective approach to derive the surface permeability and intracrystalline diffusivity via commonly used uptake/release rate measurements. Essentially, the intracrystalline diffusivity is intrinsic to the properties of guest molecules and the topological structure of host materials, while the surface permeability is sensitive to the non-ideality of a surface owing to the physical and chemical properties, host-guest interaction at surface and the change of environment. In this sense, our proposed method can directly reflect the sources of mass transfer constraints, and thus favor the improvement of design and synthesis of nanoporous materials.

By use of this method, we find some discrepancies between theoretical and experimental results concerning the intracrystalline diffusivity of guest molecules could be clarified. We show that the intracrystalline diffusivity of guest molecules in nanoporous crystalline materials is independent of measurement techniques, crystal size, and external surface properties, which is consistent with the theoretical and MD simulation results. In this regard, our method can unify the theory and experiments concerning the molecule transport in nanoporous crystalline materials.

Meanwhile, it should highlight that the surface barriers have a fundamental role in limiting mass transport of guest molecules in nanoporous materials. By use of our proposed method, the physical insight of surface barriers can be revealed. For example, we show that the concentration of external acidity and host-guest interaction at surface of SAPO zeolites can have direct influence on the surface permeability. Furthermore, the explicit expression of surface permeability in this work could provide an effective and useful tool to establish correlation between surface properties and surface barriers. In summary, we expect that this work can provide a potential way to directly quantify surface permeability and intracrystalline diffusivity for mass transfer of guest molecules, which would benefit the researches and applications of nanoporous crystalline materials.

Methods

Analysis of uptake rate. With the surface permeability α determined by Eq. (3), the DRM for spherical crystal is^{22,43}

$$\frac{m_t}{m_\infty} = 1 - \sum_{n=1}^{\infty} \frac{6L^2 \exp\left(-\frac{\beta_n^2 D t}{R^2}\right)}{[\beta_n^2 + L(L-1)]\beta_n^2}; \beta_n \cot \beta_n = 1 - L = 1 - \frac{\alpha R}{D} \quad (8)$$

and for cubic crystal is^{3,43}

$$\frac{m_t}{m_\infty} = 1 - \sum_{h,m,n=1}^{\infty} \frac{8L^6 \exp\left(-\frac{4(\gamma_h^2 + \gamma_m^2 + \gamma_n^2) D t}{a^2}\right)}{(\gamma_h^2 + L^2 + L)(\gamma_m^2 + L^2 + L)(\gamma_n^2 + L^2 + L)\gamma_h \gamma_m \gamma_n}; \gamma_i \tan \gamma_i = L = \frac{\alpha a}{2D} \quad (9)$$

could be used to determine intracrystalline (transport) diffusivity.

The detailed analysis could be found in manuscript and Supplementary Information: Fig. 2, Supplementary Figs. 6, 7 (interference microscopy, IFM), Supplementary Figs. 8, 9 (intelligent gravimetric analyzer, IGA), Supplementary Fig. 10 (tapered element oscillating microbalance, TEOM), Supplementary Fig. 11 (pulsed field gradient nuclear magnetic resonance (PFG NMR)), and Supplementary Table 4 for diffusion of methanol in SAPO-34 zeolites at small molecular loading by different measured techniques; Fig. 3, Supplementary Fig. 12 and Supplementary Table 5 for uptake rate of propane in SAPO-34 zeolites with varying different crystal size measured by IGA at 313 K; Fig. 3, Supplementary Fig. 13, and Supplementary Table 6 for uptake rate of ethane and propylene in SAPO-34 zeolites measured by IGA at 313 K; Fig. 4, Supplementary Fig. 15, and Supplementary Table 7 for uptake rate of propane in SAPO-34 zeolites adsorbed by saturated water vapor for 1 day and exposed to air for different time; Fig. 4, Supplementary Fig. 15, and Supplementary Table 8 for uptake rate of propane in SAPO-34 zeolites pre-adsorbed water for different quantity; Fig. 5, Supplementary Figs. 17, 18, and Supplementary Table 9 for uptake rate of 2-methylhexane in SAPO-11 hierarchical zeolites at 288 K. The analysis of robustness of Eq. (3) could be found in Supplementary Fig. 22 and Supplementary Tables 10, 11. The application range of Eq. (3) is shown in Supplementary Fig. 1.

Experimental materials and methods. The synthesis procedure of the SAPO-34 zeolites has been reported in our previous work^{37–39}. The zeolites are named according to their crystal size (see Supplementary Fig. 4). Before experiments, the calcination was performed at 823 K for 6 h to remove the organic template. The phase structure of the SAPO-34 was characterized by X-ray diffraction (XRD) (see Supplementary Figs. 2, 3). The size and morphological features of SAPO-34 zeolites were determined by means of field-emission scanning electron microscopy (FE-SEM) (see Supplementary Fig. 4). The bulk chemical composition was analyzed by X-ray fluorescence (XRF) spectrometer (see Supplementary Table 1), and surface chemical composition was measured by energy dispersive X-ray spectroscopy (EDX) (see Supplementary Fig. 5). The external acidity of SAPO-34 zeolites was probed by pyridine adsorption was measured by Fourier transform infrared spectra (FT-IR) (see Supplementary Figs. 19–20 and Supplementary Table 3). The textural properties of SAPO-34 zeolites were measured by nitrogen adsorption and desorption isotherms at 77 K (see Supplementary Fig. 21 and Supplementary Table 2).

Data availability

The authors declare that the main data supporting the findings of this study are available within the article and Supplementary Information file. Other relevant data are available from the corresponding author upon reasonable request.

Received: 9 October 2018 Accepted: 11 March 2019

Published online: 08 April 2019

References

- Davis, M. E. Ordered porous materials for emerging applications. *Nature* **417**, 813–821 (2002).
- Weckhuysen, B. M. & Yu, J. Recent advances in zeolite chemistry and catalysis. *Chem. Soc. Rev.* **44**, 7022–7024 (2015).
- Remi, J. C. S. et al. The role of crystal diversity in understanding mass transfer in nanoporous materials. *Nat. Mater.* **15**, 401–406 (2016).
- Li, Y., Cao, H. & Yu, J. Toward a new era of designed synthesis of nanoporous zeolitic materials. *ACS Nano* **12**, 4096–4104 (2018).
- Heinke, L., Gu, Z. & Wöll, C. The surface barrier phenomenon at the loading of metal-organic frameworks. *Nat. Commun.* **5**, 4562–4567 (2014).
- Fasano, M. et al. Interplay between hydrophilicity and surface barriers on water transport in zeolite membranes. *Nat. Commun.* **7**, 12762–12769 (2016).
- Sholl, D. S. & Lively, R. P. Defects in metal-organic frameworks: challenge or opportunity? *J. Phys. Chem. Lett.* **6**, 3437–3444 (2015).
- Zhang, J. & Li, C. M. Nanoporous metals: fabrication strategies and advanced electrochemical applications in catalysis, sensing and energy systems. *Chem. Soc. Rev.* **41**, 7016–7031 (2012).
- Chiavazzo, E., Fasano, M., Asinari, P. & Decuzzi, P. Scaling behaviour for the water transport in nanoconfined geometries. *Nat. Commun.* **5**, 3565–3575 (2014).
- Gao, M. et al. A modeling study on reaction and diffusion in MTO process over SAPO-34 zeolites. *Zeolites. Chem. Eng. J.* <https://doi.org/10.1016/j.cej.2018.08.054> (2019).
- Ma, X. & Scott, T. F. Approaches and challenges in the synthesis of three-dimensional covalent-organic frameworks. *Commun. Chem.* **1**, 98–112 (2018).
- Kärger, J. et al. Microimaging of transient guest profiles to monitor mass transfer in nanoporous materials. *Nat. Mater.* **13**, 333–343 (2014).
- Chmelik, C. & Kärger, J. In situ study on molecular diffusion phenomena in nanoporous catalytic solids. *Chem. Soc. Rev.* **39**, 4864–4884 (2010).
- Krishna, R. Diffusion in porous crystalline materials. *Chem. Soc. Rev.* **41**, 3099–3118 (2012).
- Heinke, L. & Kärger, J. Correlating surface permeability with intracrystalline diffusivity in nanoporous solids. *Phys. Rev. Lett.* **106**, 074501 (2011).
- Chmelik, C. et al. Effect of surface modification on uptake rates of isobutane in MFI crystals: an infrared microscopy study. *Chem. Mater.* **19**, 6012–6019 (2007).
- Hendriks, F. C. et al. Single-molecule fluorescence microscopy reveals local diffusion coefficients in the pore network of an individual catalyst particle. *J. Am. Chem. Soc.* **139**, 13632–13635 (2017).
- Whiting, G. T., Nikolopoulos, N., Nikolopoulos, I., Chowdhury, A. D. & Weckhuysen, B. M. Visualizing pore architecture and molecular transport boundaries in catalyst bodies with fluorescent nanoprobess. *Nat. Chem.* **11**, 23–31 (2019).
- Zhang, L., et al. Direct assessment of molecular transport in mordenite: dominance of surface resistances. *Chem. Commun.* **42**, 6424–6426 (2009).
- Hibbe, F. et al. The nature of surface barriers on nanoporous solids explored by microimaging of transient guest distributions. *J. Am. Chem. Soc.* **133**, 2804–2807 (2011).
- Teixeira, A. R. et al. 2D surface structures in small zeolite MFI crystals. *Chem. Mater.* **27**, 4650–4660 (2015).
- Tanaka, S. et al. Adsorption and diffusion phenomena in crystal size engineered ZIF-8 MOF. *J. Phys. Chem. C.* **119**, 28430–28439 (2015).
- Teixeira, A. R. et al. Dominance of surface barriers in molecular transport through silicalite-1. *J. Phys. Chem. C.* **117**, 25545–25555 (2013).
- Qi, X., Vattipalli, V., Dauenhauer, P. J. & Fan, W. Silica nanoparticle mass transfer fins for MFI composite materials. *Chem. Mater.* **30**, 2353–2361 (2018).
- Jin, D. et al. Hierarchical silicoaluminophosphate catalysts with enhanced hydroisomerization selectivity by directing the orientated assembly of premanufactured building blocks. *ACS Catal.* **7**, 5887–5902 (2017).
- Vattipalli, V., Qi, X., Dauenhauer, P. J. & Fan, W. Long walks in hierarchical porous materials due to combined surface and configurational diffusion. *Chem. Mater.* **28**, 7852–7863 (2016).
- Bai, P., Haldoupis, E., Dauenhauer, P. J., Tsapatsis, M. & Siepmann, J. I. Understanding diffusion in hierarchical zeolites with house-of-cards nanosheets. *ACS Nano* **10**, 7612–7618 (2016).
- Reitmeier, S. J., Gobin, O. C., Jentys, A. & Lercher, J. A. Enhancement of sorption processes in the zeolite H-ZSM5 by postsynthetic surface modification. *Angew. Chem. Int. Ed.* **48**, 533–538 (2009).
- Wloch, J. Effect of surface etching of ZSM-5 zeolite crystals on the rate of n-hexane sorption. *Microporous Mesoporous Mater.* **62**, 81–86 (2003).
- Kortunov, P. et al. Influence of defects on the external crystal surface on molecular uptake into MFI-type zeolites. *Chem. Mater.* **16**, 3552–3558 (2004).
- Tzoulaki, D. et al. Assessing molecular transport properties of nanoporous materials by interference microscopy: remarkable effects of composition and microstructure on diffusion in the silicoaluminophosphate zeotype STA-7. *J. Am. Chem. Soc.* **132**, 11665–11670 (2010).
- Tzoulaki, D., Schmidt, W., Wilczok, U. & Kärger, J. Formation of surface barriers on silicalite-1 crystal fragments by residual water vapour as probed with isobutane by interference microscopy. *Microporous Mesoporous Mater.* **110**, 72–76 (2008).
- Zheng, S., Jentys, A. & Lercher, J. A. Xylene isomerization with surface-modified HZSM-5 zeolite catalysts: An in situ IR study. *J. Catal.* **241**, 304–311 (2006).
- Ye, G. et al. Effects of zeolite particle size and internal grain boundaries on Pt/Beta catalyzed isomerization of n-pentane. *J. Catal.* **360**, 152–159 (2018).
- Karwacki, L. et al. Morphology-dependent zeolite intergrowth structures leading to distinct internal and outer-surface molecular diffusion barriers. *Nat. Mater.* **8**, 959–965 (2009).
- Karwacki, L., Stavitski, E., Kox Marianne, H. F., Kornatowski, J. & Weckhuysen, B. M. Intergrowth structure of zeolite crystals as determined by optical and fluorescence microscopy of the template-removal process. *Angew. Chem. Int. Ed.* **46**, 7228–7231 (2007).
- Zimmermann, N. E. R., Balaji, S. P. & Keil, F. J. Surface barriers of hydrocarbon transport triggered by ideal zeolite structures. *J. Phys. Chem. C.* **116**, 3677–3683 (2012).
- Beersden, E., Dubbeldam, D. & Smit, B. Understanding diffusion in nanoporous materials. *Phys. Rev. Lett.* **96**, 044501 (2006).
- Kärger, J. Transport phenomena in nanoporous materials. *Chemphyschem* **16**, 24–51 (2015).
- Shimizu, S. & Hamada, H. Synthesis of giant zeolite crystals by a bulk-material dissolution technique. *Angew. Chem. Int. Ed.* **38**, 2725–2727 (1999).
- Schwieger, W. et al. Hierarchy concepts: classification and preparation strategies for zeolite containing materials with hierarchical porosity. *Chem. Soc. Rev.* **45**, 3353–3376 (2016).
- Crank, J. *The Mathematics of Diffusion*. (Oxford University Press, London, 1979).
- Kärger, J., Ruthven, D. M. & Theodorou, D. N. *Diffusion in Nanoporous Materials*. (Wiley-VCH, Weinheim, 2012).
- Chen, D., Rebo, H. P., Moljord, K. & Holmen, A. Methanol conversion to light olefins over SAPO-34. Sorption, diffusion, and catalytic reactions. *Ind. Eng. Chem. Res.* **38**, 4241–4249 (1999).
- Humpalik, T., Raj, R., Maroo, S. C., Laoui, T. & Wang, E. N. Effect of hydrophilic defects on water transport in MFI zeolites. *Langmuir* **30**, 6446–6453 (2014).
- Heinke, L., Kortunov, P., Tzoulaki, D. & Kärger, J. Exchange dynamics at the interface of nanoporous materials with their surroundings. *Phys. Rev. Lett.* **99**, 228301 (2007).
- Heinke, L. Significance of concentration-dependent intracrystalline diffusion and surface permeation for overall mass transfer. *Diffus. Fundam.* **4**, 1–11 (2007).
- Chen, D., Rebo, H. P. & Holmen, A. Diffusion and deactivation during methanol conversion over SAPO-34: a percolation approach. *Chem. Eng. Sci.* **54**, 3465–3473 (1999).
- Chmelik, C. et al. Mass transfer in a nanoscale material enhanced by an opposing flux. *Phys. Rev. Lett.* **104**, 085902 (2010).
- Beersden, E., Smit, B. & Dubbeldam, D. Molecular simulation of loading dependent slow diffusion in confined systems. *Phys. Rev. Lett.* **93**, 248301 (2004).
- Zimmermann, N. E. R., Smit, B. & Keil, F. J. Predicting local transport coefficients at solid-gas interfaces. *J. Phys. Chem. C.* **116**, 18878–18883 (2012).
- Hedin, N., DeMartin, G. J., Roth, W. J., Strohmaier, K. G. & Reyes, S. C. PFG NMR self-diffusion of small hydrocarbons in high silica DDR, CHA and LTA structures. *Microporous Mesoporous Mater.* **109**, 327–334 (2008).
- Guedré, L., Bats, N. & Jolimaître, E. Effect of surface resistance on cyclohexane uptake curves in Silicalite-1 crystals. *Microporous Mesoporous Mater.* **147**, 310–317 (2012).
- Müller, K., Vankova, N., Schöttner, L., Heine, T. & Heinke, L. Dissolving uptake-hindering surface defects in metal-organic frameworks. *Chem. Sci.* **10**, 153–160 (2019).
- Li, Z., Martinez-Triguero, J., Concepcion, P., Yu, J. & Corma, A. Methanol to olefins: activity and stability of nanosized SAPO-34 molecular sieves and control of selectivity by silicon distribution. *Phys. Chem. Chem. Phys.* **15**, 14670–14680 (2013).

56. Zheng, S., Heydenrych, H. R., Röger, H. P., Jentys, A. & Lercher, J. A. On the enhanced selectivity of HZSM-5 modified by chemical liquid deposition. *Top. Catal.* **22**, 101–106 (2003).
57. Yang, M. et al. A top-down approach to prepare silicoaluminophosphate molecular sieve nanocrystals with improved catalytic activity. *Chem. Commun.* **50**, 1845–1847 (2014).
58. Gao, B. et al. A low-temperature approach to synthesize low-silica SAPO-34 nanocrystals and their application in the methanol-to-olefins (MTO) reaction. *Catal. Sci. Technol.* **6**, 7569–7578 (2016).
59. Wu, P. et al. Synthesis of nanosized SAPO-34 with the assistance of bifunctional amine and seeds. *Chem. Commun.* **54**, 11160–11163 (2018).

Acknowledgements

This work is supported by the National Natural Science Foundation of China (Grant No. 91834302).

Author contributions

M.G. carried out the uptake rate measurement and zeolitic material characterization in this work; H.L. and M.G. developed and derived an explicit expression of uptake rate with surface permeability, and M.G. further implemented and applied this approach; M. G., M. Ye, and H.L. analyzed the experimental results; M. Yang, P.W. and P.T. synthesized the SAPO-34 zeolites; S.G. and S.X. performed the PFG NMR diffusion measurement; M.G., H.L., and M. Ye planned the experiments; M. Ye and Z.L. initialized and supervised the project. All authors helped in writing the paper and commented on it.

Additional information

Supplementary information accompanies this paper at <https://doi.org/10.1038/s42004-019-0144-1>.

Competing interests: The authors declare no competing interests.

Reprints and permission information is available online at <http://npg.nature.com/reprintsandpermissions/>

Publisher's note: Springer Nature remains neutral with regard to jurisdictional claims in published maps and institutional affiliations.



Open Access This article is licensed under a Creative Commons Attribution 4.0 International License, which permits use, sharing, adaptation, distribution and reproduction in any medium or format, as long as you give appropriate credit to the original author(s) and the source, provide a link to the Creative Commons license, and indicate if changes were made. The images or other third party material in this article are included in the article's Creative Commons license, unless indicated otherwise in a credit line to the material. If material is not included in the article's Creative Commons license and your intended use is not permitted by statutory regulation or exceeds the permitted use, you will need to obtain permission directly from the copyright holder. To view a copy of this license, visit <http://creativecommons.org/licenses/by/4.0/>.

© The Author(s) 2019